Korean J. Chem. Eng., 39(6), 1566-1575 (2022)
DOI: 10.1007/s11814-021-1048-1

pISSN: 0256-1115
eISSN: 1975-7220

Effective interfacially polymerized polyarylester solvent resistant nanofiltration membrane from liquefied walnut shell

Ayang Zhou*,†, Ying Wang*, Dandan Cheng, Mengying Li*, and Lei Wang*****

*School of Materials and Chemical Engineering, Chuzhou University, China
**School of Materials Science and Engineering, Tianjin Polytechnic University, Tianjin, China
***Huaibei Leike Biotechnology Co., Ltd, Huaibei, China
(*Received 3 August 2021 • Revised 22 November 2021 • Accepted 18 December 2021*)

Abstract−Walnut shell, an agricultural waste, has not been efficiently utilized so far. In this paper, walnut shell was liquefied first, followed by characterization of XPS and ATR-FTIR. It is shown that syringylphenol and guaiacylphenol are contained in the walnut shell. A novel organic solvent resistant nanofiltration (OSN) membrane was prepared by liquefied walnut shell (LWP) and trimethyl chloride (TMC) on the crosslinked polyetherimide substrate via interfacial polymerization method. The results showed that LWP and TMC formed polyarylester toplayer. The NF-2LWP membrane maintained stable N,N-Dimethylformamide (DMF) permeance of 2.2 L m^{-2} h^{-1} MPa^{-1} and rejection of 98% for crystal violet (CV, 407.98 g mol^{-1}) in 36 hours continuous separation process. Furthermore, guaiacol (GA), a component of LWP, was used to prepare an OSN membrane, Compared with NF-LWP membrane, NF-GA membrane shows good performance in the separation of tetrahydrofuran (THF) with the rejection of 96% for rose bengal (RB, 1,017.64 g mol^{-1}) and the permeance of 76 L m^{-2} h^{-1} MPa^{-1}. This study not only provides a good way for the efficient recycling of walnut shell, but also provides a new component for the preparation of polyarylester OSN membrane.

Keywords: Walnut Shell, Liquefied, Membrane, Interfacial Polymerization, Nanofiltration, Solvent Resistance

INTRODUCTION

The application scenario of nanofiltration has broadened from aqueous solution to organic solution system [1-6]. Due to the development of solvent-resistant nanofiltration membrane, the application of membrane technology in a field such as catalyst solvent recovery and the removal of dyes from organic wastewater has become technically feasible [7]. Organic solvent resistant nanofiltration, a pressure driven membrane process, can separate molecules with molecular weight in the range of 100-1,000 gmol, which has attracted much attention due to its stability in organic solvent medium. OSN has a wide range of applications, including catalyst recovery, pharmaceutical solvent recovery and lube oil dewaxing [8,9]. Since there is no phase change, the energy required in the OSN process is relatively low, compared with traditional distillation and the distillation method used in organic solvent recovery.

For instance, a biomimetic asymmetric polyamide OSN membrane fabricated via IP among TMC and a mixture of MPD and dopamine (DA) and 1H,1H,2H,2H-Per-fluorodecane-thiol (PFDT) exhibited ethanol permeance of 15.7 L m^{-2} h^{-1} MPa^{-1} as well as a high rejection of 99.5% for rose bengal (RB) dye molecules [10]. A poly[acrylate-co-amide] thin film composite (TFC) membrane was prepared by photo-polymerization, which had a permeance of 13.2 L m^{-2} h^{-1} MPa^{-1} and a rejection about 91% for sudan black B (456.54 g mol^{-1}) in THF [11]. However, polyamide nanofiltration membranes are also facing increasing challenges. Compared with the nanofiltration membrane used in water treatment, the permeance of OSN membrane still needs to be further improved. To solve these problems, new membrane materials, such as ultrathin lamellar MoS_2 membranes for organic solvent nanofiltration [12], ultrathin 2D-Layered cyclodextrin membranes [13] and metal organic framework material filtration [14] are increasingly being developed and applied. One of the new developed solvent resistant nanofiltration membranes is characterized by the selection of some phenolic materials. The polyarylate membranes prepared by these materials usually have strong solvent resistance and show excellent separation performance in polar aprotic solvents [15].

Due to the low price and easy availability of natural woody biological materials, the research and development of such materials has aroused widespread interest and concern in the world. More than 100 million tons of lignocellulosic materials are produced by photosynthesis every year, including about 100 million tons of rice, wheat and straw [16]. However, these lignocellulosic materials have not been entirely utilized for a long time due to technical and economic factors. Walnut shell, an agricultural waste, is generally used as fuel at present, which leads to its low utilization value and environmental pollution. In fact, the main components of walnut shell, such as lignin and cellulose, have not been fully utilized. Thermochemical liquefaction technology, commonly known as liquefaction, is an effective way to bring out the potential value of natural wood biological materials [17,18]. Lin et al. found that the liquefaction products of walnut shell contained lignin structure with abundant guaiacyl structural units and phenolic hydroxyl groups [19], and Zheng et al., found that walnut shell had good reaction

†To whom correspondence should be addressed.
E-mail: zhouayang@foxmail.com

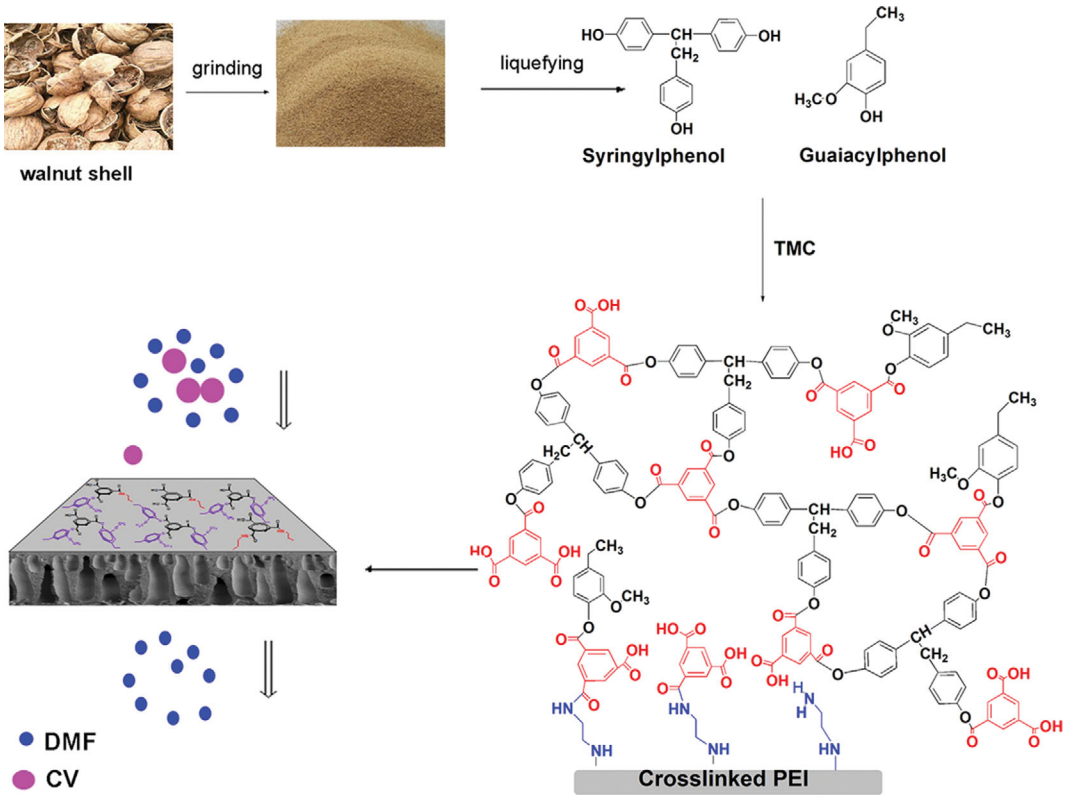

Scheme 1. A possible interfacial polymerization mechanism of syringylphenol and guaiacylphenol, the monomers, reacting with TMC.

ability with formaldehyde under alkaline conditions [20,21]. Meanwhile, lignin and its derivatives showed low solubility in many organic solvents [22], and vanillic alcohol (VA), as a model compound of lignin had been used to synthesize a thin film composite membrane, which showed stable performance in DMSO [23].

In this study, walnut shell was first liquefied with phenol as shown in Fig. S1. To prepare a solvent-resistant composite membrane used on DMF separation, the liquefied walnut shell powder, containing syringylphenol and guaiacylphenol, was used as an interfacial polymerization monomer to react with trimethyl chloride on the crosslinked polyetherimide based membrane as shown in Scheme 1. It is evaluated that the prepared membrane is resistant to organic solvents and can be stable in DMF. Moreover, to reveal the relationship between monomer and raw materials, guaiacol, a component of LWP, is used to prepare composite membrane with TMC. Compared with membrane prepared with LWP and TMC, the membrane prepared with GA and TMC shows better performance in the separation of tetrahydrofuran (THF). This study not only provides an efficient way for walnut shell utilization, but also brings out a novel route for the selection of solvent-resistant molding materials.

EXPERIMENTAL

1. Materials

The species of walnut used in this study is Yanghe walnut. The origin of this walnut is Yanghe Yi Autonomous County, Dali City, Yunnan Province, China. According to Zheng [20], in each unit structure of this rippling walnut shell lignin, the number of phenolic hydroxyl and aliphatic hydroxyl is roughly 1.24 and 2.61, respectively, and the aliphatic hydroxyl accounts for 68% of the total hydroxyl base of walnut shell. At the same time, the guaiac lignin is the main lignin, accounting for about 80% of the total lignin of walnut shell. The walnut is first ground by ball mill to 200-mesh sieve. Phenol was purchased from Shanghai Lingfeng Chemical Reagent Co., Ltd, sulfuric acid was purchased from Shanghai Bohe Fine Chemicals Co., Ltd. Polypropylene non-woven fabric was supplied by Tianjin Teda Filters Co., Ltd. Polyether imide (PEI) model Ultem 1000 as a base membrane material was supplied by Saudi Basic Industries Corporation. Ethylenediamine (EDA), dimethylacetamide (DMAc), and sodium hydroxide were supplied by Kemiou Chemical Reagent Co., Ltd (Tianjin, China). Crystal violet (CV, 407.98 g mol^{-1}) was supplied by Sinopharm Chemical Reagent Co. Ltd (China). N-dimethylformamide (DMF) was supplied by MYM Biotechnology Co., Ltd (Shanghai, China).

2. Liquefaction of Walnut Shell Powder

According to the method reported in the references [20,21], phenol and walnut shell powder was first added into a three port flask equipped with a condensing and stirring device, and heated to 100 °C in an oil bath. Then, 98% concentrated sulfuric acid catalyst was added dropwise in the stirring state, and the timing was started after the addition of sulfuric acid. The dosage of each raw reagent was: the mass ratio of walnut shell powder to phenol is 1 : 5, when the amount of sulfuric acid is 2% of the mass of phenol and the liquefaction time is 1 h, as well as the liquefaction product of walnut shell powder is prepared. After cooling of the liquefaction product, sulfuric acid was neutralized with 30% sodium

hydroxide solution, and then the solution was filtered to obtain the required interfacial polymerization monomer.

3. Preparation of Composite Membranes

3-1. Preparation of the Crosslinked PEI Support

The crosslinked PEI support was prepared according to our previous work [24]. The PEI casting solution (23 wt%) was dissolved in DMAc at 60 °C, stirred in a three-neck flask for 4 hours, and the stirring speed was controlled at 600 rpm. After removing the bubbles in the casting solution, a steel knife with a gap of 100 μm was used to scrape the casting solution onto the polypropylene non-woven fabric, and then soak it in deionized water for 1 hour. A methanol solution of 6% (w/V) EDA was added to the membrane surface to crosslink the membrane for 1 hour.

3-2. Preparation of NF-LWP Membranes

First, the surface of crosslinked PEI membrane was immersed in a mass volume ratio of 2% (w/V) LWP aqueous solution at 25 °C for 2 minutes, then the membrane surface was lightly wiped with filter paper, and 0.1% (w/V) TMC/hexane solution was poured into C-PEI surface for 1 minute. Afterward, the membrane was heated by microwave with the frequency of 2,450 MHz and output power of 1,000 W for 1 min. After being taken out, the membrane surface was cleaned with deionized water followed by refrigeration.. The membranes prepared with LWP with mass volume ratios of 0.5%, 1%, 1.5%, 2% and 4% (g/100 ml) were named NF-0.5LWP, NF-1LWP, NF-1.5LWP, NF-2LWP, and NF-4LWP, respectively. For comparison, the membranes prepared with guaiacol with mass volume ratios of 1%, 2%, 3% and 4% (g/100 ml) were prepared and named NF-1GA, NF-2GA, NF-3GA, and NF-4GA, respectively. NF-C is named as the membrane that is directly poured into TMC after crosslinked by EDA.

4. Characterization of Membrane Performance

XPS (Thermo, USA) was used to determine the element composition and identify the existence of a specific element of top layer of membrane. The surface images of a 10×10 μm^2 membrane area with morphological statistics were characterized by AFM (Seiko, Japan). The concentration of the dyes and clindamycin phosphate was analyzed with a UV-Vis spectrophotometer (METASH, China). Dynamic light scattering (DLS) analysis was performed with a Malvern Zetasizer Nano ZS. The filtration experiments of Polyethylene glycol (PEG) including PEG200, PEG400, PEG600 and PEG800, were carried out to characterize the average pore size distribution of the membrane according to the theory founded by Michaels's and Singh et al. work [25,26].

Characterization of membrane performance was carried out in a stainless steel dead-end filtration module with area of 38.5 cm^2. SEM (LEO, Germany) was used for characterization of morphology. All tests were repeated at least three times to obtain the average value and error.

The permeance (P, L m^{-2} h^{-1} MPa^{-1}) of the membrane is expressed by Eq. (1),

$$P = \frac{V}{A \times t \times \Delta p} \tag{1}$$

where V, A, t and ΔP represent the permeated volume, the membrane area, the time interval and the operating pressure, respectively.

The rejection (R) of the membrane is expressed by Eq. (2),

$$R = \left(1 - \frac{C_p}{C_f}\right) \times 100\% \tag{2}$$

where C_p and C_f represent the concentrations of the permeated solution and the feed solution, respectively.

5. UV Characterization of TMC and LWP Consumption Rate

Before UV characterization, 0.60 mL LWP solution was added to a cuvette and 0.5 mL TMC solution was also added into the cuvette. The UV-vis spectrophotometer was used to in situ monitor the absorbance change at 290 nm of the trimesoyl chloride solution and at 279 nm of carbonyl group of aromatic nucleus near the organic/aqueous interface.

RESULTS AND DISCUSSION

As shown in Fig. 1, the morphology of walnut powder before liquefaction was irregular. After liquefaction, the morphology of walnut shell powder changed greatly, showing uniform particle size. Before the liquefaction of walnut powder, the main component of walnut powder was disordered lignin structure. After liquefaction,

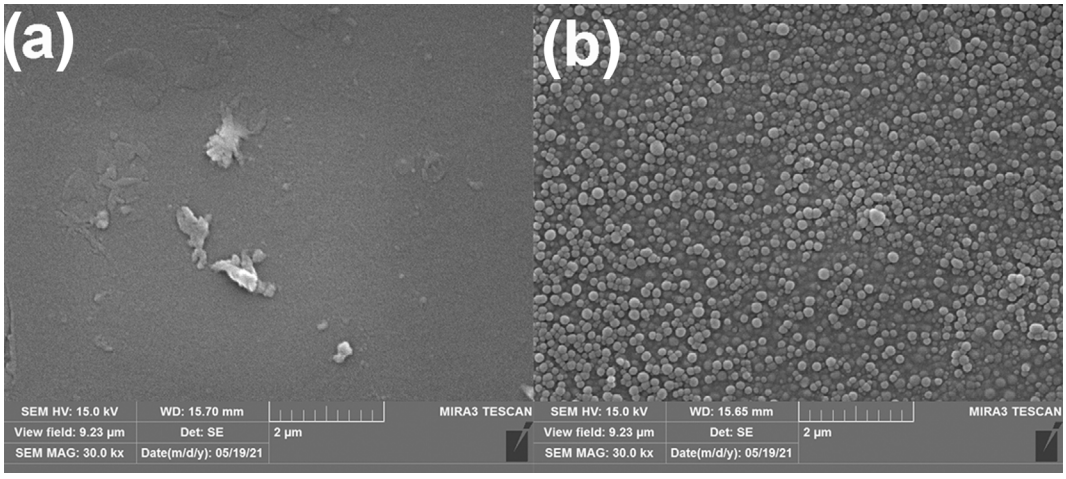

Fig. 1. (a) Walnut shell powder before liquefaction and (b) walnut powder residue after liquefaction.

the lignin structure of walnut powder broke and generated relatively uniform new phenols with low relative molecular weight. Therefore, it can be seen that the liquefied products have relatively uniform morphology in scanning electron microscope. As shown in Fig. S2, the liquefied walnut shell powder particles have a narrow size distribution presenting a peak centered at 612 nm with 556 nm of width. While walnut shell powder particles present a peak centered at 945 nm with 1,309 nm of width. Compared with that before liquefaction, the walnut shell after liquefaction has a narrower particle distribution, which is mainly due to the structural reorganization caused by hydrothermal process.

Fig. 2 displays a typical survey spectrum for fully delignified sample of liquefied walnut shell powder (LWP) and walnut shell powder (WP). According to the survey scans of XPS, all sample surfaces consist mainly of carbon, oxygen and hydrogen. After liquefaction of walnut shell, the content of carbon increased from 65.36% to 78.84%, while the content of oxygen decreased from 30.9% to 19.35% significantly, which indicates that the liquefaction is not only the dissociation of some guaiacol, but also the participation of phenol in the reaction, resulting in the formation of complex compounds containing multiple phenyl groups.

As shown in Fig. 3, the absorption peak at 1,736 cm^{-1} is C=O stretching vibration, which has the characteristic of carbonyl group. With the extension of liquefaction time, the absorption peak at 1,715 cm^{-1} is obviously enhanced, which indicates that there is a large amount of carbonyl group. The absorption peak at 1,598 cm^{-1} is the skeleton vibration of benzene ring. The absorption peaks at 1,458 cm^{-1} and 1,509 cm^{-1} are aromatic skeleton vibration. After liquefaction of walnut powder, these three absorption peaks are enhanced, indicating that a large number of benzene rings are connected, which illustrates the reaction between the product and the liquefaction reagent phenol exactly happened. At the same time, the absorption peak of phenol hydroxyl group at 3,400 cm^{-1} is also significantly enhanced, and at 1,226 cm^{-1}, the original walnut shell powder has no obvious absorption peak, The enhancement indicates that lignin is easy to condense under acidic conditions, and the absorption peak of phenolic hydroxyl at 1,366 cm^{-1} is much

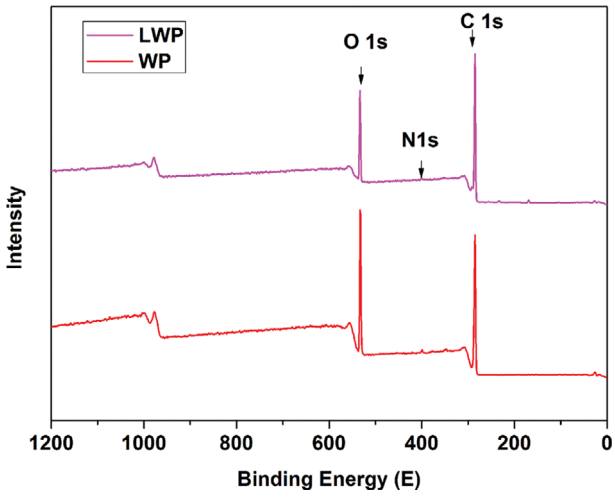

Fig. 2. Typical survey spectra and high resolution O 1s spectra for liquefied walnut shell powder (LWP) and walnut shell powder (WP).

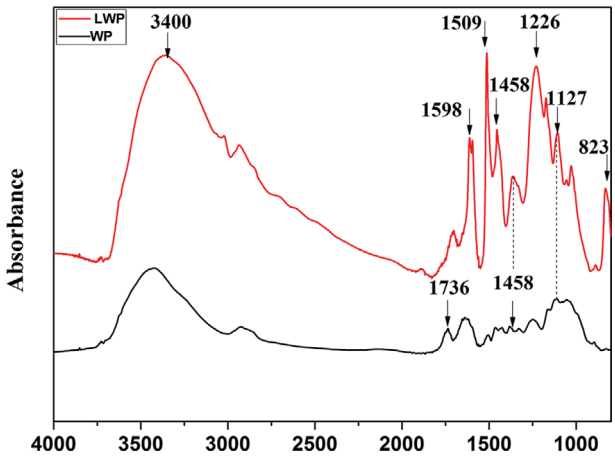

Fig. 3. FTIR spectra of liquefied walnut shell powder (LWP) and walnut shell powder (WP).

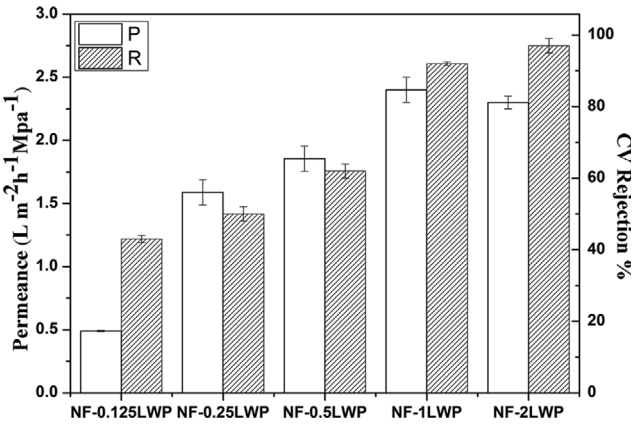

Fig. 4. The performance of membranes with different LWP concentrations (0.125%, 0.25%, 0.5%, 1%, 2% (w/v)) for a 0.01 g·L^{-1} CV in DMF solution.

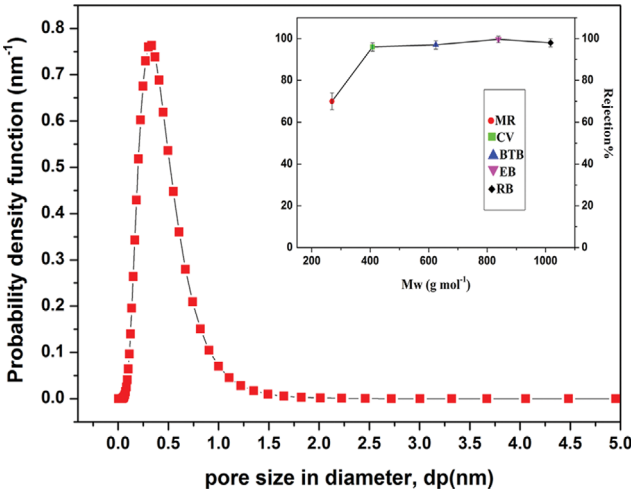

Fig. 5. Pore size distribution and molecular weight cut-off (MWCO) of NF-2LWP membrane.

stronger than that of walnut shell powder, which explains that more phenolic hydroxyl is produced. The bending vibration at 823 cm^{-1} is out of the C-H plane, which is typically located at positions 2 and 6 of guaiacol benzene ring. While 1,127 cm^{-1} is the characteristic peak of syringyl group, which is very sensitive for the detection of syringyl group [27]. Therefore, the walnut shell we used mainly belongs to guaiacyl-syringyl lignin (GS).

The performance of membranes with different LWP concentrations in separating 0.01 $g{\cdot}L^{-1}$ CV from DMF is shown in Fig. 4. The membrane NF-0.125LWP has a permeance of 0.5 L m^{-2} h^{-1} MPa^{-1} and a 43% rejection of CV. When the LWP concentration reaches 1 g, the NF-1LWP has a maximum permeance value of 2.5 L m^{-2} h^{-1} MPa^{-1} and is able to do 92% rejection of CV The membrane NF-2LWP has a maximum rejection of 98% followed by a decrease in the permeance of 2.2 L m^{-2} h^{-1} MPa^{-1}. For LWP-TMC membranes, the thickness of the top layer increases with the increase of LWP content, as shown in the SEM image in Fig. 6. With the increase of LWP concentration, the permeance coefficient of NF-2LWP decreases, which is due to the hydraulic resistance caused by the increase of surface thickness.

In addition, the pore size distribution and molecular weight cut-off (MWCO) of NF-2LWP are measured and plotted in Fig. 5. The mean pore diameter of NF-2LWP is about 0.31 nm with a MWCO of approximately 400 g mol^{-1} in water, which indicates the membrane is located in the pore size range of nanofiltration membranes.

The surface and cross-sectional morphology of LWP-TMC mem-

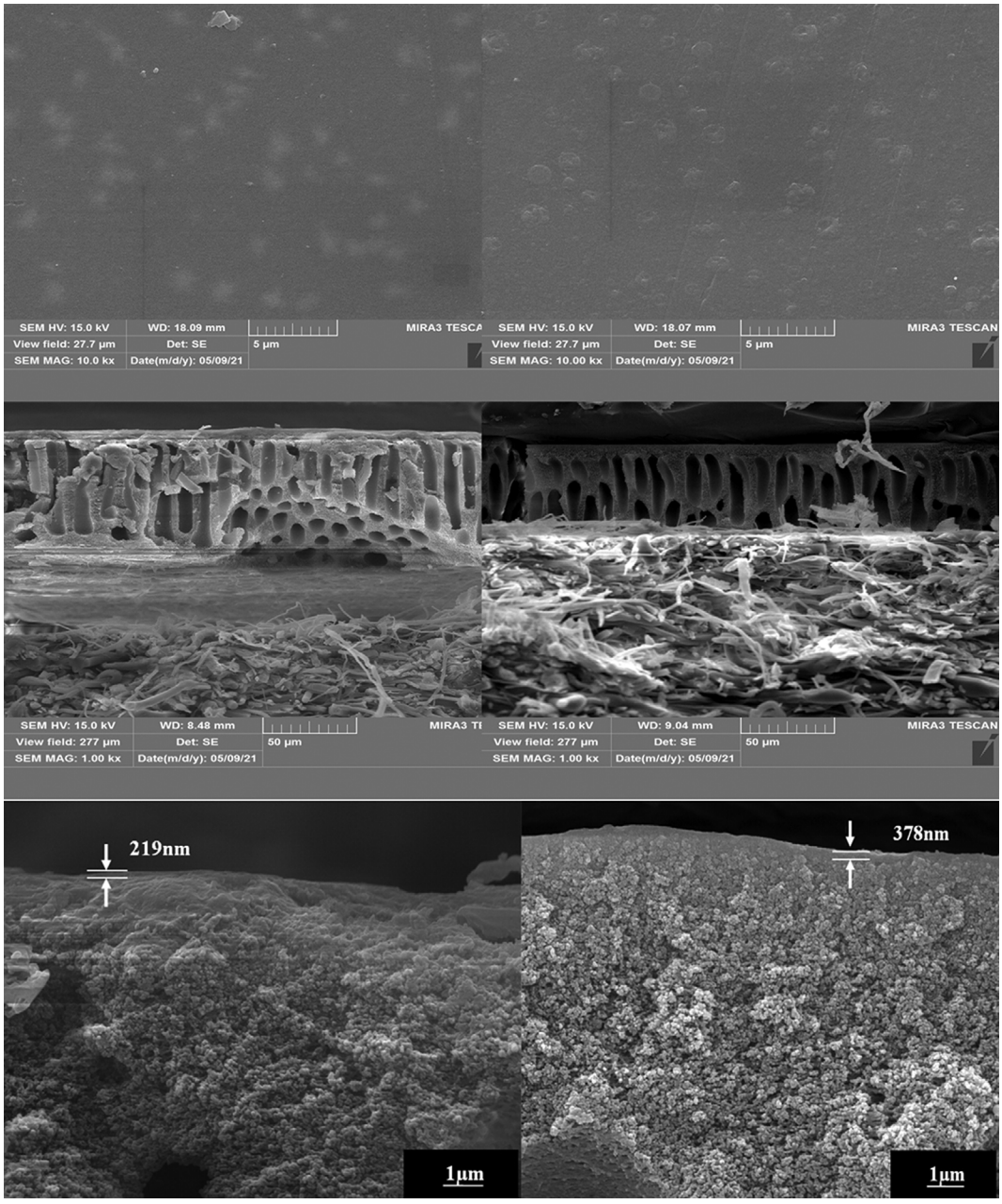

Fig. 6. SEM images of the NF-1LWP and NF-2LWP membranes.

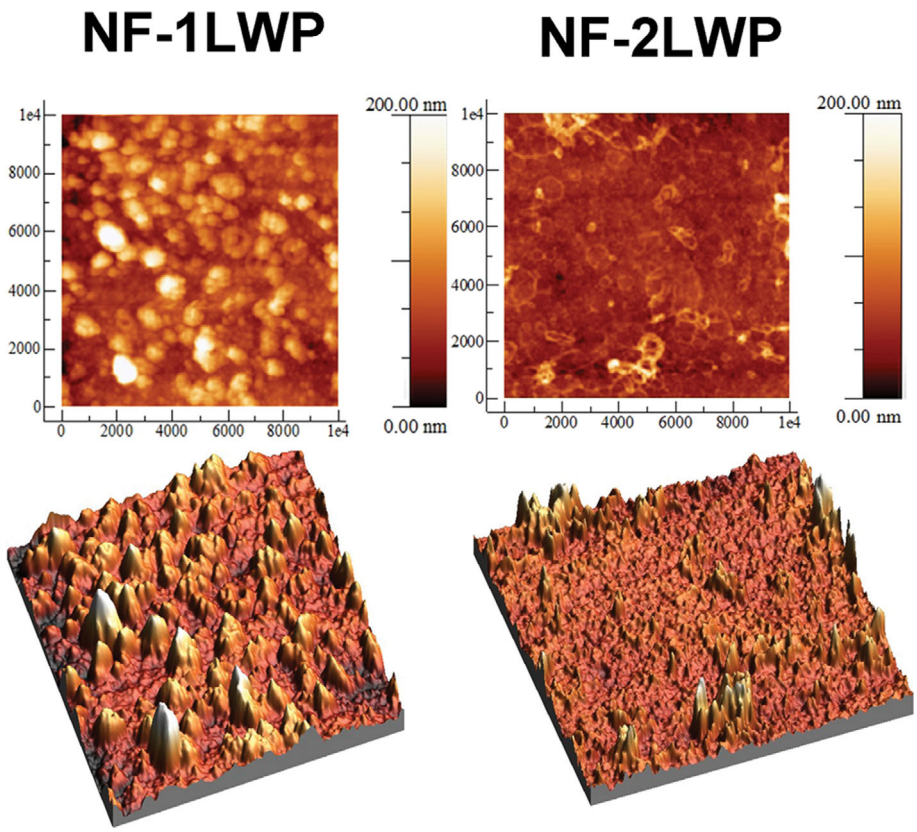

Fig. 7. Three-dimensional AFM images for NF-1LWP and NF-2LWP.

branes are shown in Fig. 6. These membranes are unsymmetrical structures composed of finger-like pore supporting layer and dense top layer. The thickness of the dense layer on top of the macrovoids is about 219 nm and 378 nm for NF-1LWP and NF-2LWP, respectively. The increase of the thickness of the top layer may be due to the increase of LWP monomer concentration.

Fig. 7 displays AFM images of the surface of NF-1LWP and NF-2LWP. The root mean square (RMS) values of surface roughness are 31.0±0.2 nm and 18±0.6 nm for NF-1LWP and NF-2LWP, respectively. This could be due to the fact that NF-2LWP has a more compact polyarylester layer than NF-LWP, which makes it smoother.

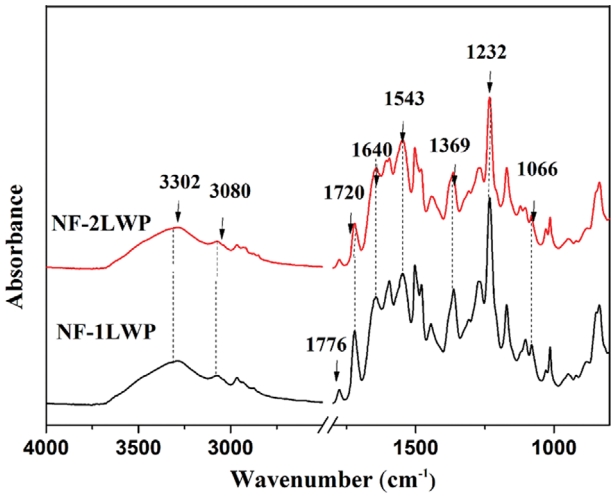

Fig. 8. The ATR-FTIR spectra of the NF-1LWP and NF-2LWP membranes.

According to Fig. 8, the spectrum for the LWP-TMC membrane displays distinct peaks located at 1,776, 1,720 and 1,369 (imide groups), 1,640 and 1,543 (amide groups) and 3,080 cm^{-1} (amine groups), respectively. For NF-1LWP and NF-2LWP, the spectra contain a series of peaks located at 3,302 cm^{-1} (hydroxyl groups), 1,066 cm^{-1} and 1,232 cm^{-1} (ester groups), respectively [28,29]. The interfacial polymerization between LWP and TMC. The calculated intensity ratio of I_{1232}/I_{1640} increases in the following order of NF-1LWP (12.5)<NF-2LWP (72.4), which illustrates more ester groups formation on the membrane surface with the increase of LWP concentration.

The deconvolution XPS C1s, N1s and O1s spectra of NF-C and NF-2LWP are obtained in Fig. S3 to distinguish carbon, nitrogen and oxygen species. For NF-C, the carbon species are located at 284.8, 285.5 and 288.1 eV, which correspond to the C-C bond of EDA, O=C- bond and C-NH bond of amide, respectively. The nitrogen species are located at 399.5, and 399.9 eV, corresponding to the -NH_2 bond of amine, O=C-NH bond of amide, respectively [30]. The oxygen species are located at 531.2 and 531.6 eV, corresponding to -OH bond of carboxylic acid groups and the O=C-NH bond of amide [31], which indicates the terminal amine groups of the C-PEI react with the TMC, forming O=C-NH bond. For

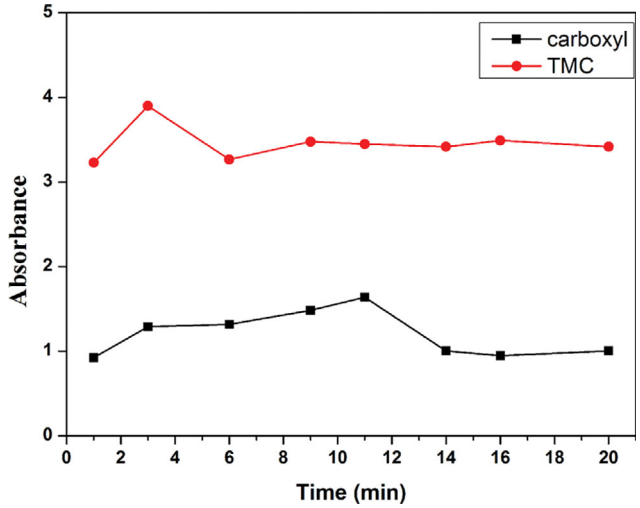

Fig. 9. UV-vis absorbance of the aqueous solution over reaction time of IP between LWP and TMC.

NF-2LWP, there is a new carbon peak at 284.9 eV and a new oxygen peak at 532.1 eV, indicating the existence of ester groups. The UV characterization further shows that the acyl chloride could polymerize with LWP. As shown in Fig. 9, the consumption rate of trimesoyl chloride and LWP in n-hexane can be obtained from the analysis of the absorbance change of UV [32]. When the acid chloride was added into the system, the intensity of the absorption peak increased first, and then the concentration of the acid chloride gradually decreased with the progress of interfacial polymerization. Due to the existence of lignin structure, LWP contains some carbonyl groups. After the addition of acyl chloride, the content of carbonyl groups in the system increased, and then decreased to the previous level with the formation of polyarylester.

As shown in Fig. 10, the water contact angle is 64±2.5° for NF-C, 36±2° for NF-0.125LWP, 41.5±2° for NF-0.25LWP, 58±1.5° for NF-0.5LWP, 71±1° for NF-1LWP and 73.5±1° for NF-2LWP. For NF-C, the chemical structure of top layer is polyamide, while the top layer of LWP-TMC membranes is polyarylester. For LWP-TMC

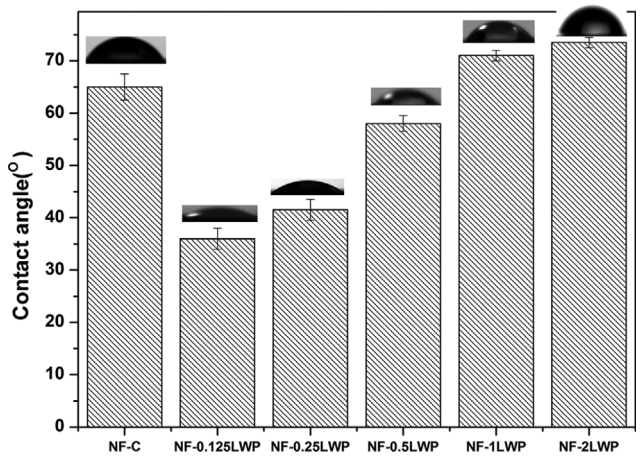

Fig. 10. The static water contact angles of NF-C, NF-0.125LWP, NF-0.25LWP, NF-0.5LWP, NF-1LWP and NF-2LWP membranes.

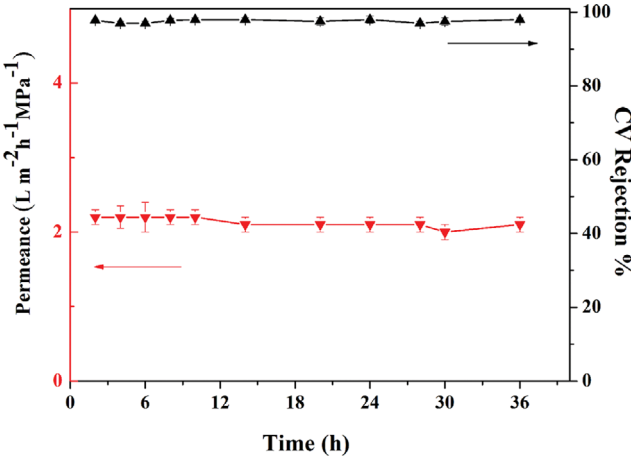

Fig. 11. The separation performance of NF-2LWP when removing CV from DMF for 36 h.

membrane, the contact angle increases with the increase of LWP concentration, which may be due to the existence of hydrophilic groups such as hydroxyl group and carboxyl group formed by the interaction of excess acyl chloride and water. However, with the increase of LWP concentration, more hydrophobic groups including methoxy groups and ester groups are formed, which leads to the increase of hydrophobicity of the membranes.

Stability test shows that the NF-2LWP membrane has stable separation performance. As shown in Fig. 11, the membrane performance is stable with a CV rejection of 98% and a permeance of approximately 2.1 L·m^{-2} h^{-1} MPa^{-1} after 36 h filtration.

Because of the excellent performance of LWP, guaiacol (GA), one of the main components of LWP, is used as the raw material to prepare the solvent-resistant composite membrane. A schematic diagram of NF-GA membrane preparation process is shown in Fig. 12.

Compared with NF-LWP, the permeance of guaiacol prepared membrane is 1.1 L m^{-2} h^{-1} MPa^{-1}, the rejection for CV is only 56%. This may be due to the fact that the membrane formed by GA and TMC cannot form a complex network structure like NF-LWP. Compared with NF-LWP, NF-GA has a larger contact angle as shown in Fig. 13, the water contact angle is 80±2° for NF-2GA, 89.5±2.5° for NF-3GA, and 90.5±2° for NF-4GA, which may be due to the fact that GA has more methoxyl groups. Note that the separation performance of solvent-resistant membrane is usually related to the polarity of the separated solvent [33]. For example, for some hydrophobic membranes, the permeability of nonpolar solvents is higher than that of polar solvents [34].

For the above reasons, NF-GA membrane is used to separate dyes in THF which has weaker polarity than DMF. RB is chosen as the separating dye which has higher solubility than CV in THF. As shown in Fig. 14, when the GA concentration reaches 3 g, the NF-3GA has a maximum permeance value of 75 L m^{-2} h^{-1} MPa^{-1} and be able to get a rejection 96% rejection of RB. The reason why there are such differences in the separation of different solvents for NF-GA and NF-LWP is related to the surface properties of the membrane, the polarity and viscosity of the solvent [35].

GA-TMC membrane also has the good solvent resistance, as

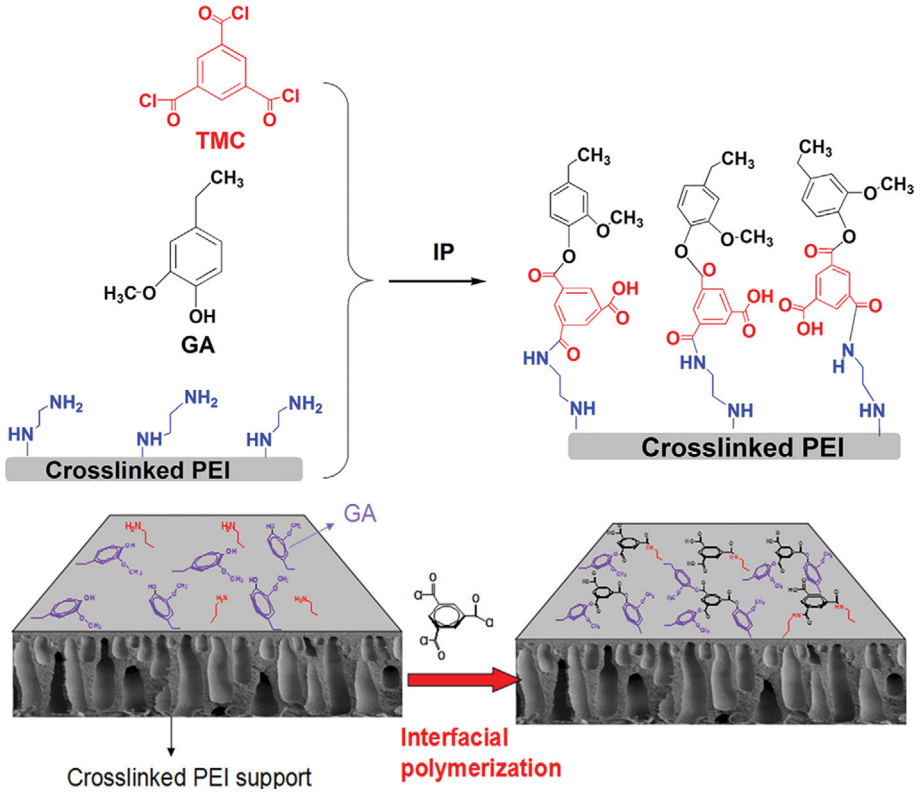

Fig. 12. Schematic diagram of preparation process of NF-GA membrane.

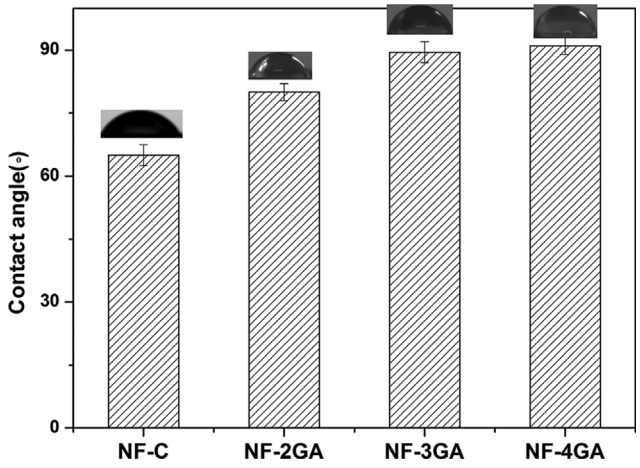

Fig. 13. The static water contact angles of NF-C, NF-2GA, NF-3GA and NF-4GA membranes.

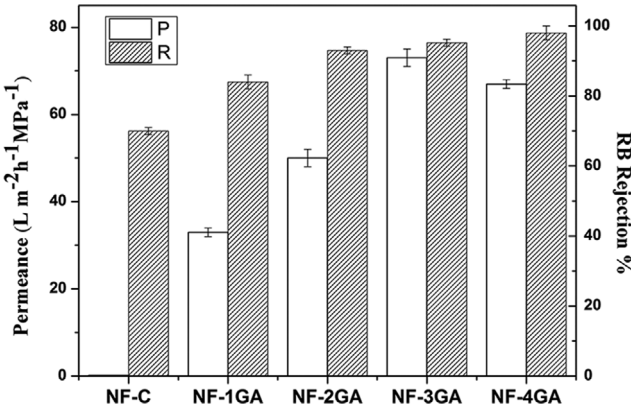

Fig. 14. The performance of membranes with different GA concentrations (0, 1%, 2%, 3%, 4% (w/v)) for a 0.01 g·L^{-1} RB in THF solution.

shown in Fig. 15, the optimal NF-3GA membrane performance is stable with an RB rejection of 96% and a permeance of approximately 76 L m^{-2} h^{-1} MPa^{-1} after 30 h filtration.

Table 1 lists the separation performance in organic solution of some polymeric membranes. For instance, Matthias et al. [36] synthesized crosslinked PVDF-membranes, showing the DMF permeance about 21.6.0 L m^{-2} h^{-1} MPa^{-1} with RB rejection of 75.0%. Shao et al. [37] used β-cyclodextrin (β-CD) and polydopamine (pDA) as the building blocks to construct OSN membranes, exhibiting the THF permeance of 6.3 L m^{-2} h^{-1} MPa^{-1} with RB rejection of 99%. Gao et al. [38] prepared a ultrathin polyethylene glycol layer via plasma method, reporting the THF permeance of 237.9 L m^{-2} h^{-1} MPa^{-1} with RB rejection of 98.5%. Thus, the synthesized NF-2LWP and NF-3GA membranes show comparable separation performance in the organic solvent of DMF and THF, respectively.

CONCLUSION

Liquefied products were selected as raw materials for preparation of solvent resistant composite membrane by IP method for the first time. The separation performance of the NF-2LWP mem-

Table 1. A comparison of OSN performance using different polymeric membranes

Membrane	Solvent permeance ($L\ m^{-2}\ h^{-1}\ MPa^{-1}$)		Solute	Mw of the solute ($g\ mol^{-1}$)	Rejection (%)	Ref.
PVDF	DMF	21.6	Rose Bengal	1,017	75	[36]
Crolsslinked-P84	DMF	16.7	Styrene oligomer	200	93	[39]
PMDA-ODA	DMF	25	Rose Bengal	1,017	96	[40]
PDA/β-CD on P84	DMF	6.3	Rose Bengal	1,017	99	[37]
PMDA-MDA	DMF	61	Rose Bengal	1,017	92	[41]
	THF	72	Rose Bengal	1,017	95	
PAH/PAA	THF	2.2	Rose Bengal	300	93	[42]
Plasma treated PEG	THF	237.9	Rose Bengal	1,017	98	[38]
PEEK on PP	THF	11	Styrene oligomers	795	90	[43]
(PIM-1/PEI)/PAN	THF	20	Hexaphenylbenzene	535	85	[44]
NF-2LWP	DMF	2.2	Crystal Violet	407	98	This work
NF-3GA	THF	75	Rose Bengal	1,017	96	
NF-4GA	THF	67	Rose Bengal	1,017	>98	

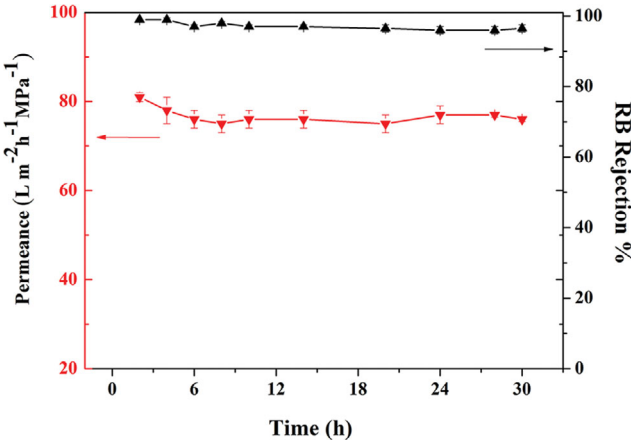

Fig. 15. The separation performance of NF-3GA when removing RB from THF for 30 h.

brane in DMF was evaluated. The results show that the membrane has significant separation performance in DMF, exhibiting rejection of 98% for CV and DMF permeance about 2.2 $L\ m^{-2}\ h^{-1}\ MPa^{-1}$. Then, guaiacol (GA), one of the main components of LWP, was used as the raw material to prepare the solvent-resistant composite membrane. The subsequent separation tests confirmed that the prepared membrane show high permeance in THF with a permeance value of 75 $L\ m^{-2}\ h^{-1}\ MPa^{-1}$ and a rejection 96% rejection of RB. This study is inspired by nature, and the synthesis process is simple and straightforward, which not only opens up an interesting research field for more natural polyphenols as OSN membrane materials, but also provides an efficient way for recycling the biomass of walnut shell.

ACKNOWLEDGEMENTS

This work was supported by National College Students Innovation and Entrepreneurship Training Program. Grant Number: 202010377024. The authors would like to thank Ze Yan for critically reviewing the manuscript.

CRediT AUTHORSHIP CONTRIBUTION STATEMENT

Ayang Zhou: Conceptualization, Resources, Writing, Supervision. Ying Wang: Software, Dandan Cheng: Formal analysis, Mengying Li: Methodology, Lei Wang.: review & editing.

DECLARATION OF COMPETING INTEREST

The authors declare that they have no known competing financial interests or personal relationships that could have appeared to influence the work reported in this paper.

ABBREVIATIONS

NF : nanofiltration
LWP : liquefied walnut shell
TMC : trimethyl chloride
AFM : atomic force microscopy
ATR-IR : attenuated total reflectance-infrared spectroscopy
DMF : N, N-dimethylformamide
DLS : dynamic light scattering
PEG : polyethylene glycol
GA : guaiacol
THF : tetrahydrofuran
SEM : scanning electron microscopy
rb : rose bengal
dmso : dimethyl sulfoxide
LWP-TMC : the membrane prepared with LWP and TMC
GA-TMC : the membrane prepared with GA and TMC

Nomenclature

A : membrane effective area [cm^2]
C_p : the concentrations of the permeated solution [kmol/kg]
C_f : the concentrations of the feed solution [kmol/kg]
FFV : membrane fraction free volume [-]

I : the calculated intensity ratio of peaks [-]
n : an integer number [-]
P : permeance of the membrane [L m^{-2} h^{-1} MPa^{-1}]
t : the time interval [h]
R : The rejection (R) of the membrane [-]
dp : pore size in diameter [nm]
Mw : molecular weight cut-off [kg/kmol]
Wavenumber : the spectrum parameter [cm^{-1}]
RMS : the root mean square [nm]
Volume : Volume distribution data [percent]
Z-Average : size distribution by dynamic light scattering [nm]
θ : the static water contact angle [°]

SUPPORTING INFORMATION

Additional information as noted in the text. This information is available via the Internet at http://www.springer.com/chemistry/journal/11814.

REFERENCES

1. N. García Doménech, F. Purcell-Milton and Y. K. Gun'ko, *Mater. Today Commun.*, **23**, 100888 (2020).
2. B. Scharzec, J. Holtkötter, J. Bianga, J. M. Dreimann, D. Vogt and M. Skiborowski, *Chem. Eng. Res. Des.*, **157**, 65 (2020).
3. Y. Zhao, T. Tong, X. Wang, S. Lin, E. M. Reid and Y. Chen, *Environ. Sci. Technol.*, **55**, 1359 (2021).
4. M. Emami, M. K. Amiri and S. Zaferani, *Korean J. Chem. Eng.*, **38**, 316 (2021).
5. S. Bandehali, A. Moghadassi, F. Parvizian and S. Hosseini, *Korean J. Chem. Eng.*, **38**, 1529 (2021).
6. M. R. Toosi, M. R. S. Emami and S. Hajian, *Environ. Sci. Pollut. R*, **25**, 20217 (2018).
7. G. Hadizade, E. Binaeian and M. R. S. Emami, *J. Mol. Liq.*, **238**, 499 (2017).
8. Y. Zhang, Q. Song, X. Liang, J. Wang, Y. Jiang and J. Liu, *Appl. Surf. Sci.*, **515**, 146005 (2020).
9. L. S. White and A. R. Nitsch, *J. Membr. Sci.*, **179**, 267 (2000).
10. B.-X. Gu, Z.-z. Liu, K. Zhang, Y.-L. Ji, Y. Zhou and C.-J. Gao, *J. Membr. Sci.*, **625**, 119112 (2021).
11. Y. Wang, J. Gu, A. Zhou, A. Kong, M. M. Alwan Almijbilee, X. Zheng, J. Zhang and W. Li, *Sep. Purif. Technol.*, **246**, 116855 (2020).
12. Y. Li, J. Li, R. B. Soria, A. Volodine and B. Van der Bruggen, *J. Membr. Sci.*, **603**, 118002 (2020).
13. T. Huang, T. Puspasari, S. P. Nunes and K.-V. Peinemann, *Adv. Funct. Mater.*, **30**, 1906797 (2020).
14. S. Yang, H. Li, X. Zhang, S. Du, J. Zhang, B. Su, X. Gao and B. Mandal, *J. Membr. Sci.*, **614**, 118433 (2020).
15. M. F. Jimenez-Solomon, Q. Song, K. E. Jelfs, M. Munoz-Ibanez and A. G. Livingston, *Nat. Mater.*, **15**, 760 (2016).
16. D. J. Tenenbaum, *Environ. Health Persp.*, **116**, 254 (2008).
17. O. Oluwasola, X. Feng, G. L. Rempel and Q. Pan, *Chem. Eng. J.*, **323**, 191 (2017).
18. D. Yue, O. Oribayo, G. L. Rempel and Q. Pan, *RSC Adv.*, **7**, 30334 (2017).
19. B. L. Lin, Y. Yao and N. Shiraishi, *Holzforschung*, **55**, 625 (2001).
20. Z. F. Zheng, J. C. Zou, B. Hua, H. J. Zhang and R. Wang, *J. Southwest For Coll*, **26**, 33 (2006).
21. Z. F. Zheng, J. C. Zou, H. J. Zhang, G. U. Ji-You and M. A. Tian-Qi, *Acta Sci. Natur. Univ. Sunyatseni.*, **46**, 139 (2007).
22. R. J. A. Gosselink, A. Abächerli, H. Semke, R. Malherbe, P. Käuper, A. Nadif and J. E. G. van Dam, *Indl. Cropand. Prod.*, **19**, 271 (2004).
23. A. Zhou, C. Shi, X. He, Y. Fu, A. W. Anjum, J. Zhang and W. Li, *Sep. Purif. Technol.*, **193**, 58 (2018).
24. X. He, A. Zhou, C. Shi, J. Zhang and W. Li, *Sep. Purif. Technol.*, **206**, 247 (2018).
25. A. S. Michaels, *Sep. Sci. Technol.*, **15**, 1305 (1980).
26. S. Singh, K. C. Khulbe, T. Matsuura and P. Ramamurthy, *J. Membr. Sci.*, **142**, 111 (1998).
27. F. Chen and C. Jiangxiang, *J. Cell Sci. Technol.*, **2**, 14 (1994).
28. S. G. Sanadhya, S. Oswal and K. C. Parmar, *J. Chem. Pharm. Res.*, **6**, 705 (2014).
29. W. Li, C. Bian, C. Fu, A. Zhou, C. Shi and J. Zhang, *J. Membr. Sci.*, **504**, 185 (2016).
30. J. Zhang, Y. Hai, Y. Zuo, Q. Jiang, C. Shi and W. Li, *J. Mater. Chem. A*, **3**, 8816 (2015).
31. W. Li, C. Bian, C. Fu, A. Zhou, C. Shi and J. Zhang, *J. Membr. Sci.*, **504**, 185 (2016).
32. C.-Y. Zhu, C. Liu, J. Yang, B.-B. Guo, H.-N. Li and Z.-K. Xu, *J. Membr. Sci.*, **627**, 119142 (2021).
33. Y. Thiermeyer, S. Blumenschein and M. Skiborowski, *Sep. Purif. Technol.*, **265**, 118492 (2021).
34. D. Bhanushali, S. Kloos, C. Kurth and D. Bhattacharyya, *J. Membr. Sci.*, **189**, 1 (2001).
35. A. Zhou, M. M. A. Almijbilee, J. Zheng and L. Wang, *Sep. Purif. Technol.*, **263**, 118394 (2021).
36. M. Matthias, V. Cédric, T. Marloes, K. Guy and I. Vankelecom, *J. Membr. Sci.*, **566**, 223 (2018).
37. Y. Zhang, H. Sun, H. Sadam, Y. Liu and L. Shao, *Chem. Eng. J.*, **371**, 535 (2019).
38. Z. F. Gao, G. M. Shi, Y. Cui and T.-S. Chung, *J. Membr. Sci.*, **565**, 169 (2018).
39. Y. H. See Toh, F. W. Lim and A. G. Livingston, *J. Membr. Sci.*, **301**, 3 (2007).
40. Y. Li, B. Cao and P. Li, *Appl. Surf. Sci.*, **473**, 1038 (2019).
41. Y. Li, J. Xue, X. Zhang, B. Cao and P. Li, *Ind. Eng. Chem. Res.*, **58**, 6712 (2019).
42. S. Ilyas, N. Joseph, A. Szymczyk, A. Volodin, K. Nijmeijer, W. M. de Vos and I. F. J. Vankelecom, *J. Membr. Sci.*, **514**, 322 (2016).
43. J. S. Burgal, L. Peeva, P. Marchetti and A. Livingston, *J. Membr. Sci.*, **493**, 524 (2015).
44. S. K. Lim, K. Goh, T.-H. Bae and R. Wang, *Chin. J. Chem. Eng.*, **25**, 1653 (2017).